ISSN 1063-7710, Acoustical Physics, 2023, Vol. 69, No. 4, pp. 448–458. © Pleiades Publishing, Ltd., 2023.
Russian Text © The Author(s), 2023, published in Akusticheskii Zhurnal, 2023, Vol. 69, No. 4, pp. 417–429.

NONLINEAR ACOUSTICS

The Use of Focused Ultrasound Beams with Shocks to Suppress Diffusion Effects in Volumetric Thermal Ablation of Biological Tissue

P. A. Pestova[a], *, M. M. Karzova[a], P. V. Yuldashev[a], and V. A. Khokhlova[a]

[a] *Moscow State University, Department of Physics, Moscow, 119991 Russia*

**e-mail: ppolina-98@yandex.ru*

Received December 21, 2022; revised March 1, 2023; accepted March 16, 2023

The article presents the results of numerical simulation of an experiment on irradiating *ex vivo* bovine liver sample by the therapeutic array of the MR-HIFU clinical system (Sonalleve V1 3.0T, Profound Medical Corp., Canada). Continuous quasi-linear and pulsed shock-wave exposures with the same time-averaged power are compared. Volumetric thermal lesions were generated by moving the focus of the array in its focal plane along discrete trajectories consisting of two or four concentric circles with a maximum radius of 4 mm. The effect of using the criteria for controlling the thermal dose during treatment and ending the sonication on the shape, volume, and exposure time of generating thermal lesion were analyzed. The acoustic field in tissue was calculated using the Westervelt equation; the temperature field was simulated with the inhomogeneous heat conduction equation; and the lesion boundary was determined according to the thermal dose threshold. In the quasi-linear mode corresponding to the clinical one, thermal diffusion leads to elongation of the lesion by a factor of 2–3 along the beam axis compared to the transverse dimension of the trajectory. The use of pulsed shock-wave exposures with switching off the inner circles of the trajectory as they reach the threshold value of the thermal dose makes it possible to significantly suppress the thermal diffusion effects in the axial direction of the beam and obtain localized thermal lesion of a given shape with a thermal ablation rate comparable to the clinical case.

Keywords: high-intensity focused ultrasound, nonlinear waves, shock front, thermal diffusion, nonlinear effects, thermal ablation, numerical simulation, thermal dose

DOI: 10.1134/S1063771023600468

INTRODUCTION

In recent decades, HIFU (high-intensity focused ultrasound) technology has been rapidly developing for noninvasive surgery, in which local destruction of affected organ tissues occurs without surgical intervention under HIFU treatment [1–4]. In clinical practice, the main mechanism of tissue destruction using HIFU is thermal ablation when the tissue is irradiated with quasi-harmonic ultrasound waves. The essence of this effect is to focus the ultrasound beam into the target zone, where the absorbed acoustic energy is converted into heat, causing thermal tissue necrosis [3, 5]. Below, thermal necrosis (ablation) caused by heating of biological tissue will be called thermal lesion or simply lesion.

To generate volumetric thermal lesion in HIFU clinical systems, a single focus of an array is sequentially moved along a specified trajectory [6, 7]. Thus, in the MR-HIFU Sonalleve V1 clinical system considered in this study, due to electronic phasing, the focus of the therapeutic array moves along discrete points located on concentric circles with radii of 2, 4, 6, and 8 mm (Fig. 1a) [6, 10 , 11]. In this case, the order of sonicating single foci on each circle is chosen such that successively irradiated points are located as far as possible from each other (shown schematically using numbering on the two inner circles in Fig. 1a). Depending on the planned size of a treatment cell, the irradiation protocol includes from one to four circles of the trajectory. If it is necessary to generate larger destruction, the transducer or irradiated region is mechanically moved to a new location and the exposure process is repeated [13].

Protocols of continuous volumetric irradiation using quasi-linear waves with acoustic power of 90–300 W are typical for HIFU clinical practice [14, 15], while each discrete focus is irradiated for tens of milliseconds (50 ms for the Sonalleve V1) [6, 11]. The generated volume of thermal ablation is controlled by built-in MRI monitoring, which displays the temperature in the irradiated zone in real time. According to the temperature growth curve in each spatial voxel of the irradiated volume, the thermal dose is calculated; then, according to its threshold value corresponding to complete tissue necrosis (240 cumulative equivalent minutes at a temperature of 43°C), the contour of the ablated region is determined [14]. Irradiation starts from the inner circle, which is repeatedly sonicated

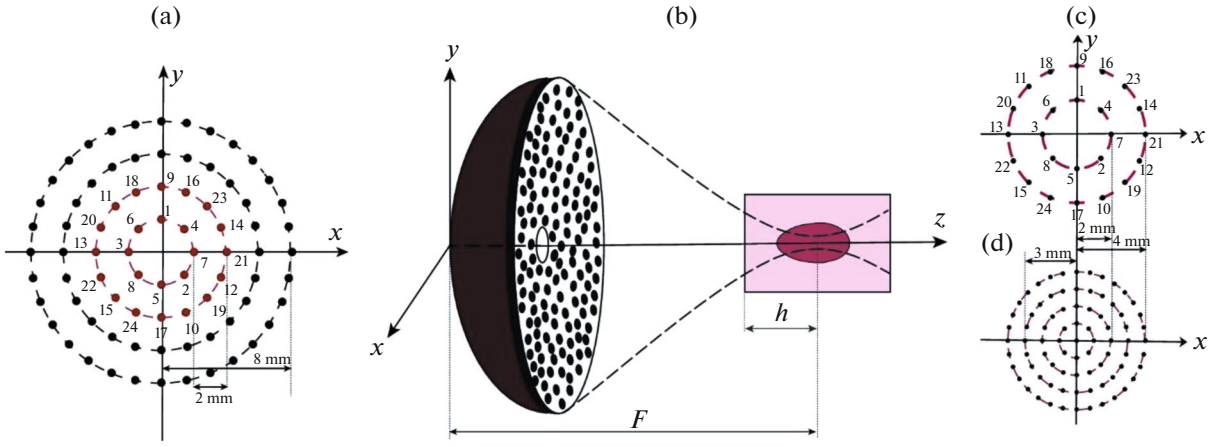

Fig. 1. (a) Clinically used treatment trajectory of a single focus movement consisting of four concentric circles with radii of 2, 4, 6, and 8 mm. The sequence of electronic steering of the transducer array focus is indicated by numerals. (b) Scheme of numerical simulation of experiment. The ultrasound beam is generated by a HIFU array consisting of 256 elements with a diameter of 6.6 mm and an operating frequency of 1.2 MHz; array diameter is 128 mm; focal length $F = 120$ mm; focusing to depth $h = 2.5$ cm in bovine liver tissue sample; the transducer and tissue sample are placed in water. (c, d) Two trajectories of discrete displacement of the ultrasound beam focus: (c) the first trajectory "2, 4 mm" consists of 2 concentric circles with radii of 2 and 4 mm, the interfocal distance on each circle is 1.56 mm; (d) the second one – "1, 2, 3, 4 mm" – of 4 circles with radii of 1, 2, 3, 4 mm, in this case, the distance between the foci on circles is reduced twofold (0.78 mm).

until the threshold thermal dose is reached on it. This is followed by multiple rounds of irradiation of the points of the next circle, and so on. Characteristic time of irradiating the entire trajectory is about several tens of seconds [6, 11, 12].

Homogeneous volumetric thermal lesion, consisting of multiple single lesions, is generated by thermal diffusion. In this case, the diffusion effects manifest themselves not only in the irradiated plane of the trajectory, but also in the axial direction of the ultrasound beam, which determines the final shape and volume of the lesion. Volumetric lesions observed in laboratory experiments and clinical practice, obtained in quasi-linear irradiation modes traditional for HIFU, have an ellipsoidal shape and are 2-3 times elongated in the axial direction compared with the transverse dimension of the trajectory [6, 11, 12, 16]. Significant elongation of the shape of the volumetric lesion along the beam axis due to diffusion effects prevents one from obtaining localized destruction and may undesirably damage critical structures close to the targeted region, such as bones or blood vessels [17–19]. The latter, in turn, carry away heat due to blood flow perfusion, which also increases the uncertainty of the final lesion shape.

To generate predictable localized lesions, it has recently been proposed to use pulsed shock-wave irradiation modes, in which an increase in the peak power of the transducer is accompanied by a decrease in the duty cycle in the sequence of pulses sent to the points of the discrete trajectory of the focus translation. In this case, the time-averaged beam power of the array remains the same as during conventional continuous irradiation in the clinical modes [20–24]. The presence of a high-amplitude shock fronts in the pressure waveform at the focus is accompanied by a sharp increase in beam energy absorption at the shocks [20–22]. The high degree of shock front focusing combined with rapid heating results in producing a single thermal lesion within milliseconds and the thermal diffusion effects in the axial direction have no time to manifest themselves [23, 24]. Consequently, mitigation of the thermal diffusion effects along the beam axis can be observed resulting in the formation of well-localized lesion of a given shape.

The aim of this work was to use a numerical experiment to compare the degree of the thermal diffusion effects during irradiation with high intensity focused ultrasound in the Sonalleve V1 clinical system in continuous quasi-linear or pulsed shock-wave exposures with the same time-average power. The paper analyzes how the initial peak ultrasound intensity under three different criteria for controlling the threshold thermal dose along the treatment trajectory affects the shape and volume of the resulting volumetric lesion in tissue and the rate of volumetric thermal ablation. The effect of the step size between the points of the discrete trajectory on the temperature field uniformity in the quasi-linear sonication regime was also studied.

FORMULATION OF THE PROBLEM

Figure 1b schematically illustrates the numerical simulation of the physical experiment *ex vivo*. The simulation was carried out for the therapeutic array of the MR-HIFU clinical system (Sonalleve V1 3.0T, Profound Medical Corp., Canada). The ultrasound transducer was a high-power phased array consisting of 256 round elements with a diameter of 6.6 mm, dis-

tributed randomly on a spherical surface with an aperture of 128 mm and a focal length $F = 120$ mm, the operating frequency was 1.2 MHz [25].

The ultrasound beam passed through the coupling medium (water) and was focused to a depth of $h = 2.5$ cm in a bovine liver sample (Fig. 1b). To obtain volumetric lesion, the focus of the transducer was moved in its focal plane ($x, y, z = F$) along a discrete trajectory consisting of foci located on concentric circles.

In this study, to simulate irradiation condition in situ common for a clinical use, the quasi-linear regime was chosen with an initial peak intensity on the array elements $I_0 = 1.2$ W/cm^2, corresponding to an initial acoustic power of the ultrasound beam of 105 W. The irradiation was continuous, and the time interval between single focus steering was 20 ms, which is the minimum possible electronic refocusing time for the Sonalleve V1. Simulations were carried out for two treatment trajectories in order to identify the influence of the step size between the points of the discrete trajectory on the temperature distributions uniformity in the tissue sample when generating thermal lesion of the same transverse size. The first trajectory was a traditional clinical trajectory and consisted of two circles with radii of 2 and 4 mm (Fig. 1c). The second trajectory was obtained by scaling the clinical trajectory spatially so that the step size between the foci was twice smaller and consisted of four circles with radii of 1, 2, 3, and 4 mm (Fig. 1d). In both trajectories, the inner circle contained eight points and eight more points were added consecutively to each subsequent circle, resulting in a total of 24 single foci on the first trajectory and 80 foci on the second trajectory. The sequence of irradiating single foci in both cases corresponded to the numbering shown in Figs. 1a,1c. The spatial steps between foci along each circle were 1.56 mm for the first and 0.78 mm for the second trajectory.

The shock-wave pulsed irradiation modes, which are enabling the reduction of axial elongation of the shape of volumetric lesion and mitigation of thermal diffusion effects, were simulated for two initial peak intensities on the array elements: $I_0 = 8$ W/cm^2 and $I_0 = 15$ W/cm^2. In these cases, to ensure the same time-averaged beam power as in the quasi-linear case (105 W), the duration of irradiation of a single focus was $t_{heat} = 3$ ms for $I_0 = 8$ W/cm^2 and $t_{heat} = 1.6$ ms for $I_0 = 15$ W/cm^2. The switching interval between single foci was the same (20 ms) as in the quasi-linear case. The shock-wave mode with an initial peak intensity on the array elements $I_0 = 8$ W/cm^2 corresponded to the case of fully developed shocks in the focal wave profile, and the case $I_0 = 15$ W/cm^2 corresponded to the saturation mode, the maximum achievable for research purposes in the Sonalleve V1. The peak acoustic powers of the array at selected levels of the initial peak intensity $I_0 = 8$ W/cm^2 and $I_0 = 15$ W/cm^2 on its elements were 700 W and 1300 W, respectively.

In shock-wave exposures, the power of heat sources is concentrated in a smaller focal region compared to the case of irradiation by quasi-harmonic waves [20]. Based on this, to simulate the process of generating volumetric thermal lesions in shock-wave regimes, the second treatment trajectory was chosen with a reduced spatial step compared to the clinical case (Fig. 1d), while a central point was added to the trajectory.

The influence of the criterion for ending the ultrasound exposure on the degree of thermal diffusion in the quasi-linear, and then in the shock-wave modes, was analyzed based on the results of simulating three irradiation protocols, which differed by the criterion for controlling the thermal dose:

Protocol 1 (clinical): each circle is irradiated until it reaches the threshold thermal dose, then the next circle is sonicated.

Protocol 2 (with inner circles turned off): irradiation begins in all circles of the trajectory; however, as the thermal dose is reached within each circle, this inner circles are sequentially turned off.

Protocol 3 (control of the thermal dose on the outer circle): all circles of the trajectory are irradiated until the dose threshold is reached on the outer circle.

From the simulation results, the values of the volumes of thermal lesion V and the rate of volumetric thermal ablation were obtained. In this case, the thermal ablation rate was calculated as the ratio of the lesion volume to the exposure time, and the lesion volume was determined after the sample cooled down over the region in which the thermal dose reached the threshold value. The cooling time in each sonication mode was determined by the time when the increase in the size of thermal lesion ceased due to the continued thermal diffusion after the end of exposure.

NUMERICAL MODEL

Ultrasound Field and Heat Sources

Ultrasound beam focusing in water, and then in bovine liver sample, was governed by the modified Westervelt equation, which takes into account nonlinear and diffraction effects, as well as absorption in tissue [22]:

$$\frac{\partial^2 p}{\partial\tau\partial z} = \frac{c_0}{2}\Delta p + \frac{\beta}{2\rho_0 c_0^3}\frac{\partial^2 p^2}{\partial\tau^2} + \frac{\delta}{2c_0^3}\frac{\partial^3 p}{\partial\tau^3} + L(p), \quad (1)$$

where $p = p(x, y, z, \tau)$ is pressure, $\Delta = \partial^2/\partial x^2 + \partial^2/\partial y^2 + \partial^2/\partial z^2$ is the Laplace operator, z is the coordinate along the beam axis, $\tau = t - z/c_0$ is the time in the accompanying coordinate system, parameters c_0, β, ρ_0 and δ are the sound speed, the nonlinearity coefficient, ambient density, and the coefficient of thermoviscous absorption in the medium, respectively. The values of the indicated

physical parameters for water were $\rho_0 = 998$ kg/m^3, $c_0 = 1485$ m/s, $\beta = 3.5$, and for bovine liver tissue $\rho_0 = 1050$ kg/m^3, $c_0 = 1580$ m/s, $\beta = 4.0$ [24, 26, 27]. The thermoviscous absorption coefficient in both media was chosen the same: $\delta = 4.33 \times 10^{-6}$ m^2/s.

In addition to thermoviscous absorption, to calculate absorption in liver tissue, the operator $L(p)$ was used, which corresponded to a linear frequency dependence of the absorption coefficient of 8.43 m^{-1} at a frequency of 1.2 MHz, and the logarithmic dispersion law $(c(f) - c_0)/c_0 = (c_0\alpha_0)/(\pi^2 f_0)\ln(f/f_0)$ [20, 22].

Westervelt equation (1) was simulated by a numerical algorithm developed earlier in [28], then repeatedly used to calculate high-power ultrasound fields of various medical transducers [22, 25, 29, 30]. To set the boundary condition, the model of an idealized Sonalleve V1 array was used [25], where, first, the boundary conditions were set on the spherical surface of the array as a uniform distribution of the vibrational velocity on its elements, and then, using the Rayleigh integral, they were transferred to the plane tangential to the center of the transducer.

The results of simulating Eq. (1) were used to determine the spatial distribution of the power density of the heat sources $Q(x, y, z)$ in liver tissue. For this, the pressure profile at each spatial point was first represented as a Fourier series expansion, then the total intensity of the wave I was calculated as the sum of the intensities of all harmonics ($N_{\text{harm}} \le 800$) with complex pressure amplitudes. The heat dissipation power Q in the medium due to wave energy absorption was calculated as the rate of decrease in intensity when calculating the operator of nonlinearity and absorption at each step dz along the array axis [24]:

$$Q(x,y,z) = -\frac{I(x,y,z+dz) - I(x,y,z)}{dz}. \qquad (2)$$

Heat sources were calculated in the nodes of a spatial mesh with transverse steps $dx = dy = 0.025$ mm, longitudinal step $dz = 0.1$ mm, and displayed in a window with dimensions of [–8, 8] mm along axes x and y and [100, 140] mm along axis z.

Temperature Field

The spatial distributions of the power density of heat sources Q obtained through acoustic calculation in tissue were used when simulating the temperature field using the inhomogeneous heat conduction equation:

$$\frac{\partial T}{\partial t} = \chi \Delta T + \frac{Q}{C_v}, \qquad (3)$$

where T is temperature, t is time, χ is the thermal diffusivity coefficient, C_v is the heat capacity of the sample, and Q is the power density of heat sources in the tissue, calculated by the Westervelt equation. The values of the physical parameters in Eq. (3) corresponded to liver tissue: $\chi = 1.93 \times 10^{-7}$ m^2/s, $C_v = 3.06 \times 10^6$ J/(m^3 °C) [22, 24, 26, 27].

The algorithm for solving Eq. (3) is described in detail in [24] and includes an analytical solution of the heat equation in the **k**-space:

$$\hat{T}(\mathbf{k},t) = \hat{T}_0(\mathbf{k})\exp\left(-4\pi^2 \boldsymbol{k}^2 \chi t\right) + \frac{\hat{Q}(\mathbf{k})}{4\pi^2 \mathbf{k}^2 \chi C_{\text{V}}}\left[1 - \exp\left(-4\pi^2 \mathbf{k}^2 \chi t\right)\right], \qquad (4)$$

where $\hat{T}(\mathbf{k},t), \hat{T}_0(\mathbf{k}), \hat{Q}(\mathbf{k})$ are the spatial Fourier spectra from the corresponding quantities $T(x,y,z,t)$, $T_0(x,y,z)$, $Q(x,y,z)$, and $T_0(x,y,z)$ is the initial temperature distribution in the considered volume. Transitions between Cartesian coordinates and the **k**-space were carried out using fast Fourier transform (FFT) operations included in the standard FFTW library in the Fortran programming language.

Heat conduction equation (3) was solved in two steps. First, the solution (4) was used to calculate the temperature field at a single focus; the calculation included its heating up to the time t_{heat} and further cooling. After the heating of a single focus was found, the volumetric thermal ablation was calculated starting from the initial temperature $T_0 = 20$°C. The linearity property of Eq. (3) made it possible to independently add a precalculated solution for the temperature field under a single exposure at different points of the trajectory with the time step of 20 ms, equal to the time of the focus translation along the irradiation trajectory, which significantly optimized the duration of calculations. After irradiation, cooling of the sample for 12 s was simulated for an initial peak intensity $I_0 = 1.2$ W/cm^2, 10 s for $I_0 = 8$ W/cm^2 and 7 s for $I_0 = 15$ W/cm^2 to account for the increase in the lesion volume due to continued thermal diffusion.

The solution for the temperature field of a single sonication was calculated with steps $dx = dy = 0.025$ mm and $dz = 0.1$ mm. Previously, it was shown that for the correct description of the temperature field in volumetric lesions, the transverse size of the numerical window of a single exposure must be at least twice the diameter of the outer circumference of the trajectory [31]. Based on this, a single exposure was calculated in a window with dimensions of [–8, 8] mm along axes x and y and [100, 140] mm along axis z. To further calculate the temperature in the case of volumetric ablation, in order to avoid the effect of frequency aliasing during FFT operations, the sizes of the spatial windows were selected so that there was no temperature increase at the window boundary. The solution for volumetric lesion was taken in the transverse window [–15, 15] mm.

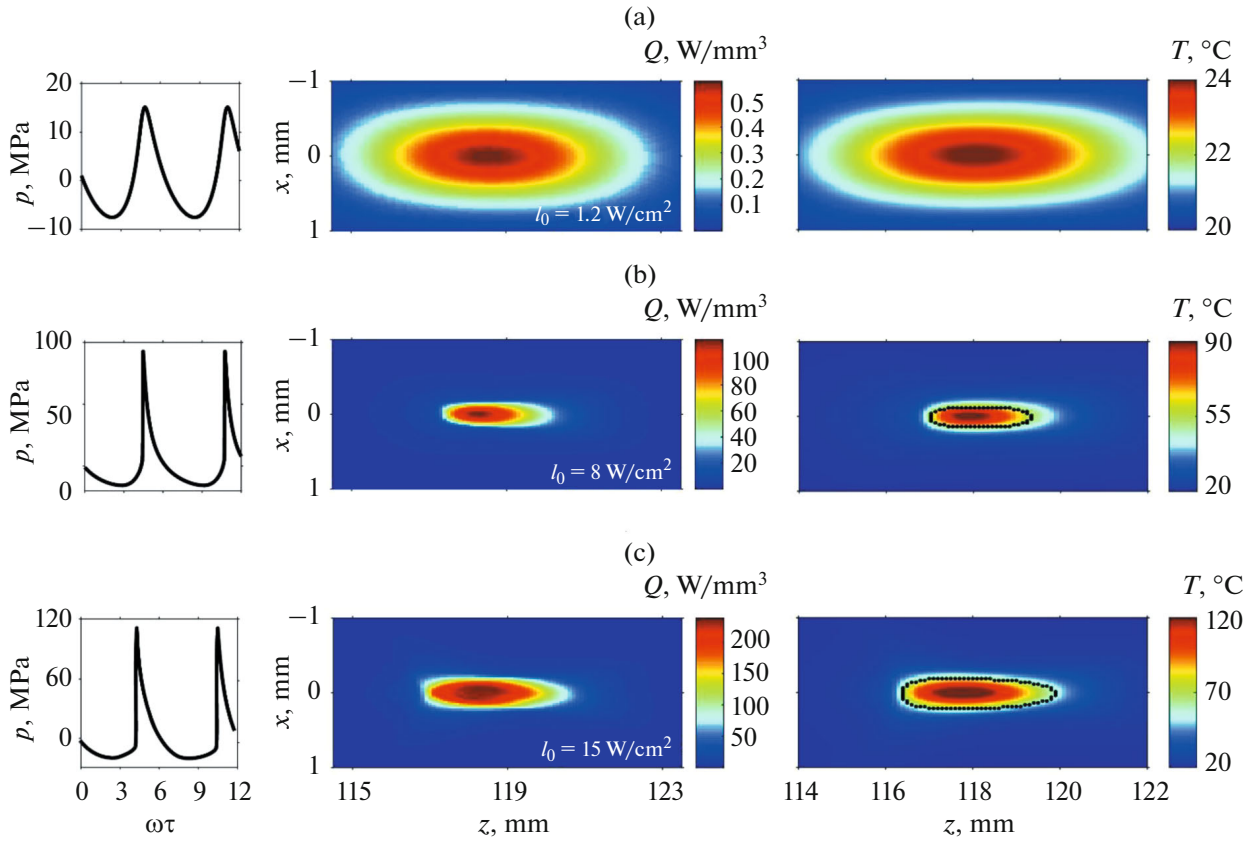

Fig. 2. Pressure waveforms at the focus (left column), spatial power density distributions of heat sources in the tissue (middle column) and temperature distributions (right column) at the moment of focus movement (20 ms) in axial (*x, z*) beam planes for the (a) quasi-linear sonication conditions with an intensity at the array elements $I_0 = 1.2$ W/cm^2, (b) regime with formation of a fully developed shock ($I_0 = 8$ W/cm^2), and (c) saturation mode ($I_0 = 15$ W/cm^2). The black contour indicates the area where the thermal dose exceeded its threshold value after the sample cooled down.

Thermal Dose

As the criterion for thermal tissue necrosis, the integral value of the thermal dose was used:

$$t_{56.0} = \int_0^{t_{\text{heat}}} R_0^{56.0-T(r,t)} dt \geq 1.76, \qquad (5)$$

where the coefficient R_0 takes a value of 0.5 for $T(\mathbf{r},t) \geq 43$°C and 0.25 for $T(\mathbf{r},t) < 43$°C [32], $t_{56.0}$ is commonly used in HIFU studies, the time equivalent to the threshold destructive thermal dose, which is 240 min at a temperature of 43°C, and 1.76 s if it is determined for a temperature of 56°C [1, 14, 24, 33]. A detailed algorithm for simulating the thermal dose is described in [24]. The spatial windows used in calculating the distribution of a single thermal dose corresponded to the spatial window used when calculating the temperature distribution at a single focus.

RESULTS

1. Acoustic Field

Figures 2a–2c (left column) show the pressure profiles calculated with Westervelt equation (1) at the focus of the HIFU array, which correspond to the initial peak intensities on its elements (a) $I_0 = 1.2$ W/cm^2, (b) $I_0 = 8$ W/cm^2, (c) $I_0 = 15$ W/cm^2 when focusing at the center of the liver tissue sample at a depth of 2.5 cm.

The mode with an initial intensity $I_0 = 1.2$ W/cm^2 corresponds to quasi-linear propagation, determined by the criterion of transitioning less than 10% of the wave energy into higher harmonics at the transducer focus [34]. In this case, an asymmetry is already present in the wave profile: the level of the peak positive pressure becomes higher than of the peak negative pressure; however, nonlinear effects are not yet significant for the extra thermal effect (Fig. 2a). As the peak intensity on the array elements increases, the focal wave profile is distorted with the subsequent formation of a shock front, and the shocks begin to form in the upper parts of the profile, then the lower boundary

of the shocks gradually shift "downward" and enters the region of negative pressure [35]. At the initial peak intensity $I_0 = 8$ W/cm^2, the lower boundary of the shock front is located near the zero pressure level (Fig. 2b), which is a distinctive feature of the so-called fully developed shock [36]. The case of formation of a fully developed shock is interesting because for it, the ratio of the shock amplitude A_{sh} (pressure jump at the shock front) to the initial amplitude of the wave pressure on the transducer p_0 reaches its maximum; i.e., focusing is the most efficient [36]. In this case, the value of the shock amplitude and the peak positive pressure are equal. With a further increase of intensity at the array elements, the increase in the ratio A_{sh}/p_0 slows down toward the onset of the saturation mode ($I_0 = 15$ W/cm^2, Fig. 2c) [37].

For initial peak intensities $I_0 = 8$ W/cm^2 and $I_0 = 15$ W/cm^2, the shock amplitudes were $A_{sh} = 90$ MPa and $A_{sh} = 120$ MPa, respectively. The theoretical estimate of the time-to-boil in tissue $t_{boil} = \left(6\rho_0^2 c_0^4 C_V \Delta T\right) \Big/ \left(\beta f_0 A_{sh}^3\right)$ for the tissue parameters used in the calculation and shock amplitudes attained is $t_{boil} = 2.9$ ms for $I_0 = 8$ W/cm^2 and 1.2 ms for $I_0 = 15$ W/cm^2. Thus, in the shock wave irradiation modes considered in this study, boiling in tissue and the concomitant formation of thermal lesions should be expected already within the heating time t_{heat} of a single focus.

The power density distributions of heat sources Q (Fig. 2, middle column) differ significantly in the case of quasi-linear heating (Fig. 2a) and shock-wave modes (Figs. 2b, 2c). The maximum Q value in the case of a fully developed shock is 200 times higher than the corresponding value in the quasi-linear case, and in the saturation mode, the analogous ratio increases up to 414 times.

In all three cases, refraction of the ultrasound beam at the water–tissue interface shifts the maximum of the field from the geometric focus $F = 120$ mm towards the transducer by 2 mm. The transverse and axial dimensions of the heat spot, calculated at the level e^{-1} from the peak value, are 1.2 mm × 1.2 mm × 7 mm for the quasi-linear heating (Fig. 2a, middle column) and significantly exceed the corresponding dimensions for the shock-wave modes (Figs. 2b, 2c, middle column). In the case of fully developed shock formation, $I_0 = 8$ W/cm^2, acoustic energy absorption by tissue is localized in a very small volume (only 0.3 mm × 0.3 mm × 2.7 mm at the level e^{-1} of the peak value). This localization is explained by the presence of shock fronts in the wave profile, which lead to sharp focusing of the acoustic field and efficient acoustic energy absorption in a small focal region. However, with further increase in the intensity at the transducer array elements, the shock front is formed in a larger focal region, which increases the area of enhanced heat sources (Fig. 2c). The characteristic dimensions of the heat spot for the saturation mode $I_0 = 15$ W/cm^2 are 0.4 mm × 0.4 mm ×3.6 mm. Thus, a non-monotonic change in the size of the region of increased wave energy absorption is observed. It is important to note that, unlike boiling histotripsy applications [31, 36, 38], where the high amplitude of the shock-wave front plays the main role, generating thermal HIFU lesions in shock-wave modes is also significantly influenced by the volume around the focus in which shocks has formed.

2. Temperature Field of a Single Exposure

Numerical simulation of the heat conduction equation (3) using solution (4) showed that for sonication of a single focus in the quasilinear mode, heating of the sample from the initial temperature $T_0 = 20$°C is about 4°C in the current single focus by the time the next irradiation starts (20 ms); as well, the thermal dose threshold is not reached at any point (Fig. 2a, right column). In shock-wave modes, residual heating by the time of 20 ms is 93°C and 126°C for $I_0 = 8$ W/cm^2 and $I_0 = 15$ W/cm^2 (Fig. 2b, c, right column), respectively, and the sizes of temperature spots replicate the corresponding dimensions of the heat sources. In this case, during electronic translation of the array focus, single thermal lesions are produced with dimensions of 0.25 mm × 0.25 mm × 2.3 mm and 0.4 mm × 0.4 mm × 3.5 mm for $I_0 = 8$ and $I_0 = 15$ W/cm^2, respectively (Figs. 2b, 2c, right column).

Thus, sharper focusing of shock fronts, accompanied by efficient acoustic energy absorption, makes it possible to obtain a fast single predictable localized thermal lesion with small size and insignificant thermal diffusion effects.

3. Obtaining Volumetric Lesion in the Quasilinear Irradiation Mode

Figure 3 shows the results of tissue volume ablation in the quasi-linear mode using the traditional clinical trajectory of two circles with radii of 2 and 4 mm in the form of spatial temperature distributions at the end of heating for the three exposure protocols described above.

In case of the exposure according to the protocol 1, which is used in clinical practice, achieving the thermal dose threshold required performing 41 repetition of sonication of the internal circumference (2 mm) first and then irradiating the external circumference (4 mm) 24 times. Within an exposure time of 14.24 s, the lesion shape in the axial direction was asymmetrically elongated due to the thermal diffusion effects: the axial size of the ablated volume after cooling was 16.8 mm, which is 2.4 times greater than the axial size of a single thermal lesion (7 mm), and the thermal ablation rate was 2.2 cm^3/min, which corresponds to the known numerical and experimental data [12, 39].

In the other two protocols, sonication along the trajectory begins the same way: two circles are irradiated in turn 30 times until the threshold value of the thermal dose on the inner circle is reached. Then, in protocol 2, movement of the focus along the inner circle was excluded and the outer circle was irradiated five more times until the thermal dose threshold was reached on it. In protocol 3, the thermal dose was controlled only on the outer circle, so irradiation continued along the entire trajectory. As a result, a total of four more rounds were made along the external circle and five along the inner one. In this case, additional exposure to the central region after the formation of thermal necrosis in it leads to overheating of the central region of the lesion and increased mean temperature in the lesion compared to the clinical protocol (63°C vs. 59°C). The consequence of this is the achievement of a larger lesion volume with more symmetrical shape and higher thermal ablation rate compared to irradiation according to the other protocols (Table 1, column "trajectory 2, 4 mm").

The assumption about the benefit of overheating the center of the treatment cell to increase the rate of tissue thermal ablation has been discussed earlier in [6, 11]. Qualitatively, this assumption can be explained by the fact that most of the heating time (about 10 s) there is a gradual heating of a given volume until a thermal lesion is formed, i.e. on this time interval, the "instantaneous rate" of thermal ablation is equal to zero. Then, as the temperature rises to 56°C–58°C, thermal ablation of a given volume occurs in seconds. In this case, an increase in the exposure time to already heated or even destroyed area is effective from the point of view of the ablation rate, since ablation of the neighboring preheated area due to thermal diffusion occurs. Taking into account the geometry of the problem, the central region of the trajectory is subject to the greatest influence of thermal diffusion when exposed to different points of the trajectory; therefore, its overheating in combination with a longer irradiation time of a given volume increases the ablation rate.

Reducing the spatial step between single foci by half while maintaining the maximum transverse size of the trajectory resulted in more uniform heating of the irradiated area for each of the three exposure protocols (Fig. 4). For irradiation according to the protocol 3, the most significant differences in the peak temperature and shape were observed: the peak temperature increased from 68 to 82°C (on average for the region from 63 to 70°C), thermal lesion had more symmetrical ellipsoidal shape, and there was an increase in the ablation volume (817 mm^3 vs. 651 mm^3) and thermal ablation rate (2.8 cm^3/min vs. 2.4 cm^3/min).

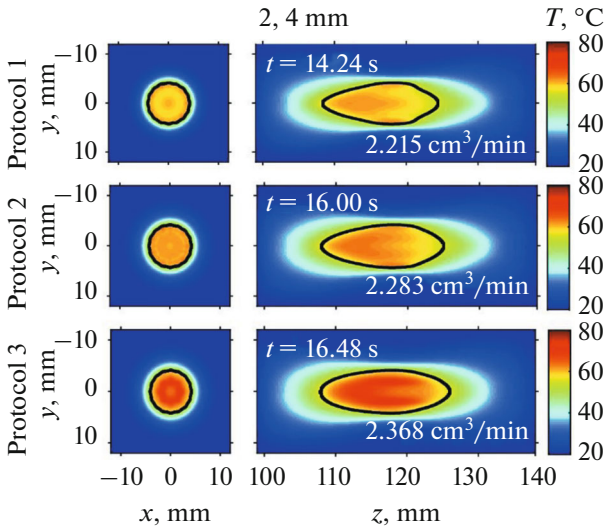

Fig. 3. Spatial temperature distributions during irradiation along a trajectory consisting of two circles with radii of 2.4 mm at the end of tissue sonication at the initial intensity I_0 = 1.2 W/cm^2. The black contour indicates the area where the thermal dose exceeded its threshold value after the sample cooled down. The top row corresponds to the "clinical" protocol; the middle row, to the "inner circle off" protocol; and the bottom row describes the "outer circle thermal dose control" protocol. Each spatial temperature distribution shows the end time of heating and the achieved rate of volumetric thermal ablation.

Analysis of the number of rounds N_i along each circle of the trajectories (Table 1) showed that clinical protocol 1 is characterized by a decrease in N_i as the

Table 1. Sonication parameters of the sample of bovine liver tissue in the quasi-linear mode with an initial peak intensity at the array elements I_0 = 1.2 W/cm^2 on circular trajectories for 3 protocols. N_i is the number of complete passes around a circle with a radius i mm. The thermal ablation rate was calculated as the ratio of the resulting lesion volume to the exposure time. V is the final volume of the lesion

I_0 = 1.2 W/cm^2	Trajectory 2, 4 mm; step 2 mm				Trajectory 1, 2, 3, 4 mm; step 1 mm					
	N_2	N_4	rate, cm^3/min	V, mm^3	N_1	N_2	N_3	N_4	rate, cm^3/min	V, mm^3
Protocol 1	41	24	2.215	526	11	9	8	8	2.270	514
Protocol 2	30	35	2.283	610	7	7	9	13	2.284	566
Protocol 3	35	34	2.368	651	11	11	11	11	2.787	817

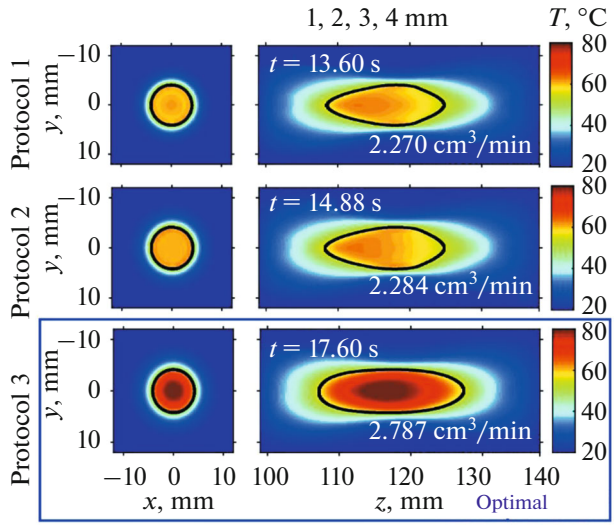

Fig. 4. Spatial temperature distributions during irradiation along a trajectory consisting of four circles with radii of 1, 2, 3, 4 mm at the end of tissue irradiation at an initial intensity $I_0 = 1.2$ W/cm^2. The description of the figure is similar to the caption to Fig. 3.

size of the circle increases, which is explained by the thermal diffusion effects. The opposite trend is observed for protocol 2 and for protocol 3, the number of passes N_i is the same for all circles.

In terms of volumetric thermal ablation rate and the size of the resulting thermal lesion, protocol 3, which uses the second treatment trajectory with a reduced spatial step, proved to be the most advantageous for the quasi-linear case (Table 1, "trajectory 1, 2, 3, 4 mm"). Compared to the clinical case (protocol 1, "trajectory 2, 4 mm"), the rate gain was 26%, and the lesion volume increased by 55%.

It is also noteworthy that an analogue of protocol 3, which consists of successive irradiation of all trajectory points and repeated repetition of such complete sonications, is used in the clinical Sonalleve HIFU system for hyperthermia, where the objective is to uniformly maintain a temperature of 40–45°C within a given volume for a long time, typically for around an hour [13].

Thus, the results of the numerical experiment showed that (1) when tissue is irradiated by quasi-linear waves, thermal diffusion plays a significant role in the formation of the final shape of volumetric thermal lesion along the transducer axis; (2) a decrease in the spatial step of the trajectory makes it possible to obtain more uniform heating; (3) for the quasi-linear sonication mode, the most advantageous protocol in terms of the thermal ablation rate and obtaining a symmetrical lesion shape is the protocol in which all trajectory points are irradiated until the threshold thermal dose on the outer circle is reached.

However, the use of the quasi-linear mode, regardless of the irradiation protocol, inevitably leads to elongation of the lesion shape by two to three times along the axis of the ultrasound beam compared to the dimensions of individual heat sources. This makes impossible the generation of predictable axially localized volumetric thermal lesions and may damage nearby critical structures.

4. Obtaining Volumetric Lesion in Shock-Wave Irradiation Modes

To suppress elongation of the shape of volumetric lesions and concomitant creation of thin, well-localized destruction, in this work, the shock-wave pulsed sonication exposures were considered. Since, in contrast to traditional quasi-linear HIFU modes, shock-wave sonication enables the attainment of a single lesion of a small size as a result of a single exposure (Figs. 2b, 2c), to, consideration of a trajectory with a reduced spatial step is a priori the most advantageous for suppressing the thermal diffusion effects. The simulation results of tissue irradiation for two shock-wave modes with initial peak intensities of 8 and 15 W/cm^2 along the trajectory with a reduced step are shown in Fig. 5 for the three previously considered protocols.

In the case of the fully developed shock ($I_0 =$ 8 W/cm^2), protocol 3, which is the most advantageous for the quasi-linear case, was the least optimal (Fig. 5, bottom row, left) in terms of localization of thermal lesion: its shape is elongated in the axial direction by 3.8 times compared to the corresponding size of a single lesion (8.8 mm vs. 2.3 mm). As well, additional overheating of the central region still leads to the highest thermal ablation rate (Table 2, column 8); however, it does not meet the objective of suppressing the thermal diffusion effects. In the other two protocols (1, 2), the inner circle is irradiated a fewer number of times, as a result of which the shape is not "stretched" (Fig. 5, upper and middle rows). The influence of thermal diffusion effects is significantly suppressed: the axial size of the volumetric lesion (3.2 mm) is only 1.4 times larger than the corresponding axial size of a single lesion (Fig. 2b), and the lesion shape becomes more localized and predictable compared to the quasilinear case. At the same time, the thermal ablation rate during irradiation according to protocol 2 was higher than in the case of protocol 1, and the lesion margins were smoother.

In the saturation mode with an initial peak intensity of 15 W/cm^2, absorption of the ultrasound beam energy by the formed shocks occurs in a region larger than the heat sources, which correspond to the case $I_0 = 8$ W/cm^2; therefore, to obtain volumetric thermal ablation, a shorter exposure time and smaller number of rounds along the trajectory circles are required (Table 2). It is also noteworthy that, depending on the protocol, either the inner or outer circle is irradiated

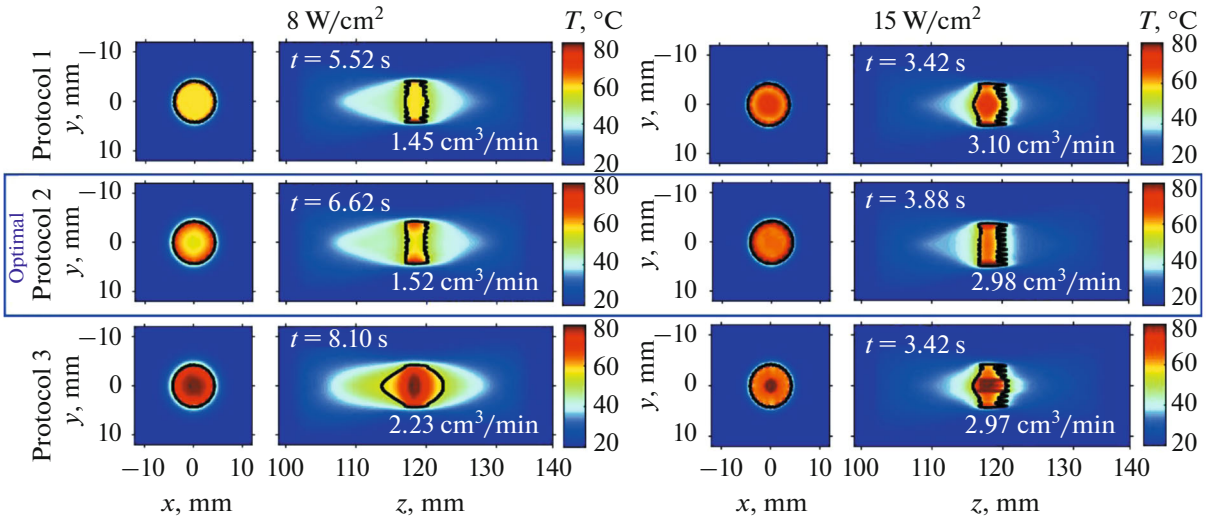

Fig. 5. Spatial temperature distributions for shock-wave irradiation with an initial peak intensity at the array elements of 8 W/cm^2 (left) and 15 W/cm^2 (right) along a trajectory consisting of 4 circles with radii of 1, 2, 3, 4 mm. The description of the figure is similar to the caption to Fig. 3.

three times in total, and the rest, two times each (Table 2, column 15). This results in similarity of the shape of lesion obtained in protocols 1 and 3 with triple irradiation of the inner circle, as well as a qualitative difference in lesion in the case of protocol 2, which was most advantageous for shock-wave exposure (Fig. 5, right). Protocol 2 made it possible to suppress "stretching" of the shape of volumetric lesion and reduce the effect of thermal diffusion. Thus, the calculation results show that the axial size of volumetric lesion (3.6 mm) replicates the corresponding size (3.5 mm) of a single lesion. Switching off the inner circles in protocol 2 during irradiation led to a more uniform temperature distribution without overheating the central region observed in protocols 1, 3.

Comparison of two shock-wave pulsed irradiation modes with initial peak intensities of 8 W/cm^2 and 15 W/cm^2 showed that with an increase in the initial peak intensity at the transducer array elements, the thermal ablation rate increases and the manifestation of the thermal diffusion effects from the heated area into the surrounding tissue layers in the axial direction decreases. For both irradiation modes, protocol 2 is the most advantageous, which enables to obtain volumetric lesions predictable in shape with sharp edges and straight front boundaries. In this case, the volume of the resulting lesions, the exposure time, and the thermal ablation rate were, respectively, 167 mm^3, 6.62 s and 1.52 cm^3/min for I_0 = 8 W/cm^2 and 192 mm^3, 3.88 s and 2.98 cm^3/min for I_0 = 15 W/cm^2. It should be noted that in the considered saturation mode (15 W/cm^2), the thermal ablation rate was twofold higher than the corresponding rate in the mode with the fully developed shocks (8 W/cm^2) and 1.4 times higher than in clinical quasi-linear mode (1.2 W/cm^2). Therefore, sonication in saturation mode is the most advantageous.

Table 2. Parameters of the bovine liver tissue sample irradiation for shock-wave pulsed sonication conditions with initial peak intensities I_0 = 8 W/cm^2 and I_0 = 15 W/cm^2 for 3 irradiation protocols. The transducer focus moved along a circular trajectory consisting of four circles with radii of 1, 2, 3, and 4 mm. N_i is the number of complete passes around a circle with a radius i mm. The thermal ablation rate was calculated as the ratio of the resulting lesion to the exposure time. V is the final volume of the lesion

I_0, W/cm^2	8						15					
	N_1	N_2	N_3	N_4	rate, cm^3/min	V, mm^3	N_1	N_2	N_3	N_4	rate, cm^3/min	V, mm^3
Protocol 1	3	3	4	3	1.45	133	3	2	2	2	3.10	179
Protocol 2	3	3	4	5	1.52	167	2	2	2	3	2.98	192
Protocol 3	5	5	5	5	2.23	302	3	2	2	2	2.97	169

To conclude, it has been demonstrated that the use of pulsed shock-wave irradiation modes with switching off the inner circles of the trajectory as the thermal dose threshold value is reached on them, enables to mitigate the thermal diffusion effects along the axis of the ultrasound beam and obtain well-localized thermal lesions of a given shape with ablation rates comparable to clinical case. For the clinical system Sonalleve V1, the implementation of such irradiation seems to be the most advantageous when using the system's maximum peak power levels.

CONCLUSIONS

Based on the obtained results, the following conclusions can be made:

(1) the quasi-linear mode (105 W), which is typical for clinical practice *in situ* for the HIFU system considered in this study, regardless of the irradiation protocol, leads to elongation of the thermal lesion along the beam axis by a factor of 2.5 vs. the axial dimension of heat sources and the transverse dimension of the trajectory; the maximum thermal ablation rate and largest lesion volume are achieved when sonicating along a trajectory with a reduced step (1 mm) and controlling the thermal dose only on the outer circumference.

(2) In shock-wave pulsed modes (peak powers 700 W and 1300 W) due to fast heating, elongation of the volumetric thermal lesion along the beam axis is suppressed; the thermal ablation rate during irradiation along a trajectory with a reduced step (1 mm) increases by 1.4 times (1300 W) compared to the clinical quasi-linear mode, and it is preferable to control the thermal dose on each circle of the trajectory, switching off the inner circles as they reach the threshold dose value.

(3) When choosing a shock-wave sonication mode, it is important to consider the region around the focus where shocks are formed , since the size of a single lesion plays a significant role in suppressing the thermal diffusion effects. In the clinical HIFU system Sonalleve V1, the greatest acceleration of thermal ablation and the most predictable localized thermal destruction with sharp edges are attained in the shock-wave mode with the highest achievable peak power.

The study demonstrates the potential of using shock-wave modes for the rapid generation of predictable and localized thermal volumetric lesions in biological tissue with suppressed effect of thermal diffusion along the transducer axis compared to the quasi-linear case. In modes that mimic clinical settings, to obtain symmetrical volumetric lesions of approximately 1 cm^3 with the highest ablation rate, it is most advantageous to control the threshold value of the thermal dose on the outer circumference of the treatment trajectory.

To quickly obtain a well-localized small lesion volume (0.2 cm^3) in the form of a layer with a thickness of about 4 mm, it is recommended to sonicate the tissue in the shock-wave mode along a trajectory with a reduced step and switching off the inner circles when controlling the thermal dose. This approach makes it possible to obtain predictable shapes of thermal lesions with sharp edges. However, despite effectively suppressing thermal diffusion in the axial direction, the formation of volumetric lesion resulting from the merging of single foci in the transverse direction still occurs due to thermal diffusion. This aspect will be taken into account in further studies, which aim to investigate irradiation along a trajectory of various geometry uniformly filled with foci with a single shock-wave sonication on each focal point. In addition, for the creation of a volumetric thermal lesion comparable in size to the clinical one (several cm^3), it seems promising to develop shock-wave protocols for layer-by-layer tissue irradiation.

As practical recommendations, it follows from the results of this study that irradiation of biological tissues in a pulsed shock-wave mode using the maximum achievable peak power of a HIFU transducer has significant advantages and can be implemented in the existing Sonalleve HIFU clinical setup. Also, this result can be generalized to other clinical HIFU systems similar to the Sonalleve.

ACKNOWLEDGMENTS

The authors are grateful to L.R. Gavrilov for valuable comments during the discussion of the results.

FUNDING

The study was supported by the Russian Science Foundation, grant no. 22-72-00047.

REFERENCES

1. *Physical Principles of Medical Ultrasonics,* Ed. by C. R. Hill, J. C. Bamber, G. R. ter Haar (John Wiley & Sons, 2004; Fizmatlit, Moscow, 2008).
2. L. R. Gavrilov, *Focused High Intensive Ultrasound in Medicine* (Fazis, Moscow, 2013) [in Russian].
3. M. R. Bailey, V. A. Khokhlova, O. A. Sapozhnikov, S. G. Kargl, and L. A. Crum, Acoust. Phys. **49** (4), 369 (2003).
4. T. J. Dubinsky, C. Cuevas, M. K. Dighe, O. Kolokythas, and J. H. Hwang, AJR, Am. J. Roentgenol. **19**, 191 (2008).
5. F. Wu, Z. B. Wang, W. Z. Chen, W. Wang, Y. Gui, M. Zhang, G. Zheng, Y. Zhou, G. Xu, M. Li, C. Zhang, H. Ye, and R. Feng, Ultrason. Sonochem. **11**, 149 (2004).
6. M. O. Köhler, C. Mougenot, B. Quesson, E. J. Enholm, B. Le Bail, C. Laurent, C. T. W. Moonen, and G. J. Ehnholm, Med. Phys. **36** (8), 3521 (2009).

7. R. Salomir, J. Palussière, F. C. Vimeux, J. A. de Zwart, B. Quesson, M. Gauchet, P. Lelong, J. Pergrale, N. Grenier, and C. T. W. Moonen, J. Magn. Reson. Imag. **12**, 571 (2000).
8. C. Mougenot, R. Salomir, J. Palussiere, N. Grenier, and C. T. W. Moonen, Magn. Reson. Med. **52**, 1005 (2004).
9. V. A. Khokhlova, A. D. Maxwell, T. Khokhlova, W. Kreider, M. Bailey, A. Partanen, N. Farr, and O. A. Sapozhnikov, in *Proc. 14th Int. Symp. for Therapeutic Ultrasound* (Las Vegas, 2014).
10. P. Ramaekers, M. De Greef, J. M. M. Van Breugel, C. T. W. Moonen, and M. Ries, Phys. Med. Biol. **61**, 1057 (2016).
11. J. K. Enholm, M. O. Köhler, B. Quesson, C. Mougenot, C. T. Moonen, and S. D. Sokka, IEEE Trans. Biomed. Eng. **57** (1), 103 (2010).
12. Y. S. Kim, B. Keserci, A. Partanen, H. Rhim, H. K. Lim, M. J. Park, and M. O. Köhler, Eur. J. Radiol. **81** (11), 3652 (2012).
13. M. Tillander, S. Hokland, J. Koskela, H. Dam, N. P. Andersen, M. Pedersen, K. Tanderup, M. Ylihautala, and M. Köhler, Med. Phys. **43** (3), 1539 (2016).
14. A. M. Venkatesan, A. Partanen, T. K. Pulanic, M. R. Dreher, J. Fischer, R. K. Zurawin, R. Muthupillai, S. Sokka, H. J. Nieminen, N. Sinaii, M. Merino, B. J. Wood, and P. Stratton, J. Vasc. Interv. Radiol. **23** (6), 786 (2012).
15. S. L. Giles, G. Imseeh, I. Rivens, G. R. Ter Haar, A. Taylor, and N. M. deSouza, J. Interv. Radiol. **3** (1:1), 1 (2020).
16. O. A. Sapozhnikov, T. D. Khokhlova, W. Kreider, A. Partanen, Y.-N. Wang, M. M. Karzova, and V. A. Khokhlova, in *Proc. 19th Int. Society for Therapeutic Ultrasound (ISTU) and the European Focused Ultrasound Charitable Society (EUFUS)* (Barcelona, 2019).
17. C. Mougenot, M. O. Köhler, J. Enholm, B. Quesson, and C. Moonen, Med. Phys. **38**, 272 (2011).
18. B. Quesson, M. Merle, M. O. Kohler, C. Mougenot, S. Roujol, B. D. de Senneville, and C. T. Moonen, Med. Phys. **37** (6), 2533 (2010).
19. J.-F. Aubry, M. Pernot, F. Marquet, M. Tanter, and M. Fink, Phys. Med. Biol. **53** (11), 2937 (2008).
20. E. Filonenko and V. A. Khokhlova, Acoust. Phys. **47** (4), 541 (2001).
21. V. A. Khokhlova, M. R. Bailey, J. A. Reed, B. W. Cunitz, P. J. Kaczkowski, and L. A. Crum, J. Acoust. Soc. Am. **119** (3), 1834 (2006).
22. P. Yuldashev, S. Shmeleva, S. Ilyin, O. Sapozhnikov, L. Gavrilov, and V. Khokhlova, Phys. Med. Biol. **58** (8), 2537 (2013).
23. V. A. Khokhlova, *Focused Ultrasound Foundation Final Report* (June 5, 2019).
24. Yu. S. Andriyakhina, M. M. Karzova, P. V. Yuldashev, and V. A. Khokhlova, Acoust. Phys. **65** (2), 141 (2019).
25. W. Kreider, P. V. Yuldashev, O. A. Sapozhnikov, N. Farr, A. Partanen, M. R. Bailey, and V. A. Khokhlova, IEEE Trans. Ultrason. Ferroelectr. Freq. Control **60** (8), 1683 (2013).
26. F. A. Duck, *Physical Properties of Tissue* (Acad. Press, London, 1990).
27. https://itis.swiss/virtual-population/tissue-properties/database/acoustic-properties/.
28. P. V. Yuldashev and V. A. Khokhlova, Acoust. Phys. **57** (3), 334 (2011).
29. M. M. Karzova, P. V. Yuldashev, O. A. Sapozhnikov, V. A. Khokhlova, B. W. Cunitz, W. Kreider, and M. R. Bailey, J. Acoust. Soc. Am. **141** (4), 2327 (2017).
30. A. D. Maxwell, P. V. Yuldashev, W. Kreider, T. D. Khokhlova, G. R. Schade, T. L. Hall, O. A. Sapozhnikov, M. R. Bailey, and V. A. Khokhlova, IEEE Trans. Ultrason. Ferroelectr. Freq. Control **64** (10), 1542 (2017).
31. P. A. Pestova, M. M. Karzova, P. V. Yuldashev, W. Kreider, and V. A. Khokhlova, Acoust. Phys. **67** (3), 250 (2021).
32. S. A. Sapareto and W. C. Dewey, Int. J. Radiat. Oncol. Biol. Phys. **10** (6), 787 (1984).
33. X. Fan and K. Hynynen, Ultrasound Med. Biol. **22** (4), 471 (1996).
34. Ultrasonics-Field Characterization-In Situ Exposure Estimation in Finite-Amplitude Ultrasonic Beams, document IEC/TS 61949 (2007).
35. P. V. Yuldashev, M. M. Karzova, W. Kreider, P. B. Rosnitskiy, O. A. Sapozhnikov, and V. A. Khokhlova, IEEE Trans. Ultrason. Ferroelect. Freq. Control **68** (9), 2837 (2021).
36. P. B. Rosnitskiy, P. V. Yuldashev, O. A. Sapozhnikov, A. D. Maxwell, W. Kreider, M. R. Bailey, and V. A. Khokhlova, IEEE Trans. Ultrason. Ferroelect. Freq. Control **64** (2), 374 (2017).
37. M. M. Karzova, M. V. Averiyanov, O. A. Sapozhnikov, and V. A. Khokhlova, Acoust. Phys. **58** (1), 81 (2012).
38. V. A. Khokhlova, J. B. Fowlkes, W. W. Roberts, G. R. Schade, Z. Xu, T. D. Khokhlova, T. L. Hall, A. D. Maxwell, Y. N. Wang, and C. C. Cain, Int. J. Hyperthermia **31** (2), 145 (2015).
39. M. M. Karzova, W. Kreider, A. Partanen, O. A. Sapozhnikov, T. D. Khokhlova, P. V. Yuldashev, and V. A. Khokhlova, in *Proc. 19th Int. Symp. of ISTU / 5th European Symp. of EUFUS* (Barcelona, 2019), p. 235.